

# Variational Autoencoders for Anomalous Jet Tagging

Taoli Cheng

*Mila – Quebec Artificial Intelligence Institute  
6666 St-Urbain, #200, Montreal, QC, H2S 3H1, Canada and  
Department of Informatics, Université de Montréal*

Jean-François Arguin, Julien Leissner-Martin, Jacinthe Pilette

*Département de physique, Université de Montréal  
Complexe des Sciences, Case postale 6128,  
succursale Centre-ville, Montréal (Québec) H3C 3J7, Canada*

Tobias Golling

*Department of Particle Physics, University of Geneva  
24, quai Ernest-Ansermet, CH-1211 Genève 4, Switzerland*

## Abstract

We present a detailed study on Variational Autoencoders (VAEs) for anomalous jet tagging at the Large Hadron Collider. By taking in low-level jet constituents' information, and only training with background QCD jets in an unsupervised manner, the VAE is able to encode important information for reconstructing jets, while learning an expressive posterior distribution in the latent space. When using the VAE as an anomaly detector, we present different approaches to detect anomalies: directly comparing in the input space or, instead, working in the latent space. Different anomaly metrics are examined. A comprehensive series of test sets are generated to fully examine the anomalous tagging performance in different jet types. In order to facilitate general search approaches such as bump-hunt, mass-decorrelated VAEs based on distance correlation regularization are also studied. Confronted with the problem of mis-assigning higher probability to out-of-distribution samples, we explore one potential solution – Outlier Exposure (OE), in which outlier samples are utilized to guide the learning heuristics. OE, in the context of jet tagging, is employed to achieve two goals at the same time: increasing sensitivity of outlier detection and decorrelating jet mass from the anomaly score. We observe excellent results from both aspects. Code implementation can be found at [Github](#).

## I. INTRODUCTION

Supervised classifiers that are based on deep neural networks have been used for boosted jet tagging and have become a mature research topic in the past few years. At the same time, it's also worth exploring other methods beyond the specific supervised taggers. The goal is to tag new physics signals in a model-independent manner in the hope of simple execution and high performance. For model-dependent new physics searches, only null results have been obtained so far at the LHC. At the same time, model-independent and data-driven methods, especially assisted by modern machine learning approaches, are becoming potential alternative search strategies. In particular, unsupervised learning methods has become more popular in the area of new physics search at the LHC. Unsupervised learning methods including clustering, density estimation, etc. have been used in the general scope of detecting novel or anomalous events. Anomaly detection methods for LHC physics [1–11] including density estimation, weakly-supervised classification, etc. have been studied recently.

Transitioning from traditional density-based or distance-based anomaly detection, deep generative models succeed in modeling complex high-dimensional density distributions, and are thus used to process high-dimensional data. We can utilize unsupervised training of deep generative models for anomalous jet tagging, while taking in all low-level features, and being as model-independent as possible.

Autoencoders (AEs) and Variational Autoencoders (VAEs) have been explored for new physics searches recently. Especially, autoencoder-based anomaly detection has been used in anti-QCD jet tagging [12–15]. Variational Autoencoders are also explored for event selection at the LHC [16]. Some of them are working on high-level features, while others are working on low-level jet constituents instead. These models are trained only with background data, and at test time are used to detect signals as anomalies. For anomalous jet tagging, autoencoders trained with only QCD jets are used to detect non-QCD jets such as boosted top jets. Autoencoders employ a bottleneck architecture to effectively reduce the data dimensionality, and by using the bottleneck, extract relevant information for reconstructing input features. Using either images or four-vector-based input features, autoencoders have been shown to be potential in detecting heavy resonances. The basic idea of using autoencoders as anomaly detector is assuming that the trained AEs will be able to reconstruct samples

similar to training samples (*in-distribution*, InD), while giving large reconstruction errors when applied to unseen datasets (*out-of-distribution*, OoD). Thus the reconstruction error is used as the anomaly score in most of the literature to date. At the same time, adversarial training to decorrelate jet mass from the reconstruction error has been explored to assist bump-hunt based new physics searches [12]. In Fig. 1, we depict the schematic of AE-based anomalous jet tagger. Jet reconstruction is encouraged by minimizing the reconstruction error between input and output samples. The latent space of deterministic AEs is not taken as optimization target, thus is not ready for direct use and has random/unregularized behaviour (see the illustrative latent distribution of QCD samples in Fig. 1). A simple idea of regularizing the latent space will lead us to the Variational Autoencoders [17]. Migrating from deterministic Autoencoders to Variational Autoencoders for anomalous jet tagging, there are a few motives: regularized and expressive latent representations, combination with generative modeling, and a framework for maximum likelihood estimation. As indicated in Fig. 2, VAE has a regularized latent distribution imposed by minimizing a divergence in latent space, in addition to minimizing the reconstruction error in input space as in the case of deterministic AEs.

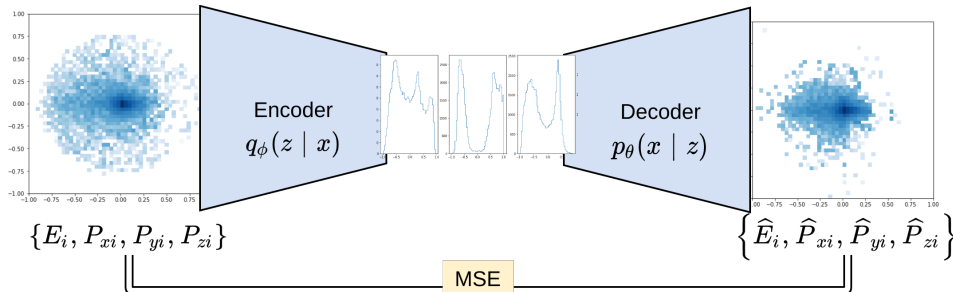


FIG. 1: Schematic of Autoencoder-based anomalous jet tagger. Jet reconstruction is encouraged by minimizing the reconstruction error between outputs  $\{\hat{E}_i, \hat{P}_{xi}, \hat{P}_{yi}, \hat{P}_{zi}\}$  and inputs  $\{E_i, P_{xi}, P_{yi}, P_{zi}\}$ .

Despite the fact that generative models provide us a simple approach for dealing with high-dimensional anomaly detection, they are not guaranteed to succeed for all the use cases. For instance, in the context of anti-QCD tagging, QCD jets might be assigned larger reconstruction error or lower likelihood than  $W$  jets with two-prong structure, as will be shown later. These problems are also encountered in the general domain of anomaly detection in

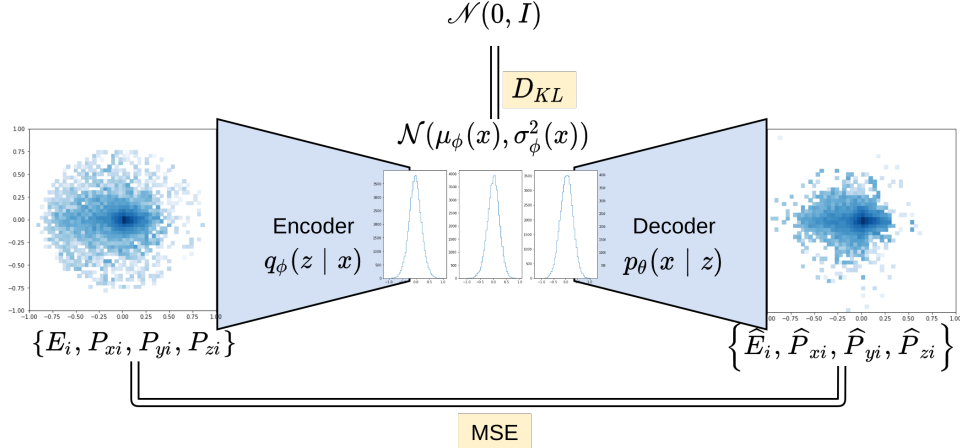


FIG. 2: Schematic of Variational Autoencoder based anomalous jet tagger. Both the reconstruction error between outputs and inputs and the divergence of latent distributions are required to be optimized.

the machine learning community. In anomaly detection of natural images, it was found that sometimes higher probability is assigned to out-of-distribution samples than in-distribution samples [18, 19]. The pixel-space similarity is still not mature enough to render robust representation learning. And sometimes background confounding also brings spurious correlation that handicaps the OoD detection.

In this work, we base our anomalous jet tagging investigation in the framework of VAEs, with possibilities of utilizing anomaly metrics in both input space and latent space. Based on the previously mentioned motivations and existing problems, we examine every building block in the process of using VAEs for anomalous jet tagging. We first construct a basic VAE model for low-level constituents-based jet taggers. In order to ensure that we have a fully performing generative model, we examine its reconstruction performance, generation performance, and also properties of the latent space. To have a fair assessment of the anomaly detection performance, we tailor a series of test jet sets spanning in the range of different jet masses and jet types. Other than the reconstruction loss used in corresponding deterministic AEs applications, we examine a few alternatives for anomaly metrics. In large radius jet based new physics searches such as bump-hunt, having a mass-decorrelated tagger will be beneficial. We thus implement a mass-decorrelated VAE tagger in a regularization-based approach [20], which is faster and easier to train than an auxiliary adversarial network.

Outlier Exposure (OE) [19] is proposed to solve the probability mis-assignment problem

(i.e. outliers are assigned higher probability) mentioned before. By injecting some outlier samples, it helps the autoencoder get better separation for InD samples and OoD samples. It is also reported that it generalizes to other OoD distributions. Furthermore, the auxiliary task of OE also provides us a very good handle to shape the latent data manifold tailored to our tasks. Actually, we employ outlier exposure not only as an inducer for detecting sensitivity of unseen outlier samples, but also as a tool to guide and shape the information encoded. Using outlier samples as a handle, we achieve decorrelation effects by using equivalent “planning” [21, 22] (or, reweighting samples to obtain identical distributions) in jet mass. We achieve very good mass decorrelation by matching mass distributions between the exposed outlier dataset and the in-distribution training dataset, while at the same time gaining promising sensitivity for most jet types.

The paper is organised as follows: in Section II we present the basic settings of the problem and examine the properties of trained VAE models; in Section III the performance in detecting non-QCD jets is carefully investigated; mass-decorrelated taggers are introduced and studied in Section IV; an outlier exposure solution to sensitivity and mass-decorrelation is presented in Section V; finally we summarize this work in Section VI.

## II. VARIATIONAL AUTOENCODERS FOR ANOMALOUS JET TAGGING

We provide here some mathematical foundation of VAEs [17, 23]. As briefly mentioned in the introduction, VAEs can be viewed as the regularized version of deterministic AEs by imposing latent structure with a Kullback–Leibler divergence (KL divergence,  $D_{\text{KL}}(P\|Q) = \sum_{X \in \mathcal{X}} P(X) \log \frac{P(X)}{Q(X)}$ ) from the prior distribution to the posterior distribution for latent variables. Practically speaking, a VAE, similar to an AE, consists of an encoder and a decoder, which are both parameterized with neural networks. By parameterizing the variational inference and the generative model with deep neural networks, VAEs map input data  $X$  ( $X \in \mathcal{X}$ ) into the latent space with  $Q(z|X)$  and map the latent representation  $z$  back into the input space with  $P(X|z)$ . The training objective of VAEs includes an extra term of minimizing the KL divergence between the prior  $P(z)$  and posterior  $Q(z|X)$  distributions of latent variables  $z$ . Despite the fact that VAE is a deep generative model, it trains fast by simple back-propagation with a reparameterization trick. The reparameterization instead reparameterizes the latent sampling using an extra input layer by the change of variable

$z = \mu + \sigma \odot \epsilon$  (with  $\epsilon \sim \mathcal{N}(0, I)$ ), in order to back-propagate through the stochasticity of latent sampling.

The actual objective of the VAE is to approximately maximize the log-likelihood  $\log P(X)$ , within a Bayesian inference framework. The log-likelihood of the input data distribution can be written in terms of:

$$\log P(X) - D_{\text{KL}}[Q(z|X)||P(z|X)] = \mathbb{E}_{z \sim Q}[\log P(X|z)] - D_{\text{KL}}[Q(z|X)||P(z)], \quad (1)$$

in which  $-\mathbb{E}_{z \sim Q}[\log P(X|z)]$  is empirically the reconstruction error of an autoencoder. The left-hand side of Eq. 1 is the marginal log-likelihood we want to maximize (the other divergence term can be effectively minimized in the case of a powerful encoder  $Q(z|X)$ ). The right-hand side of Eq. 1 is called the *Evidence Lower Bound* (ELBO), since it gives a lower bound of the log-likelihood. ELBO is just the VAE objective and practically the sum of the reconstruction error of the autoencoder and the distance between posterior and prior distributions in the latent space.

So empirically the training objective of the VAE can be written as the summation of the reconstruction error in the input space and the distributional distance in the latent space:

$$\mathcal{L}_{\text{VAE}} = \mathcal{L}_{\text{recon}} + \mathcal{L}_{\text{KL}} \quad (2)$$

From another point of view, VAEs can be seen as a regularized version of deterministic autoencoders. By imposing explicit constraints in the form of the latent prior distribution, we have a handle of how the latent variables behave. Then the training of VAEs includes matching the posterior to the prior distribution by minimizing the KL-divergence from prior to posterior distributions in latent space.

The encoder and decoder within a VAE serve as the inference network and the generative network respectively. The latent space from the encoding process provides the posterior latent representation. In standard VAEs, prior latent distributions are assumed to be multivariate standard Gaussian distribution  $\mathcal{N}(0, I)$ . And posteriors are estimated in the form of  $\mathcal{N}(\mu(X), \sigma^2(X))$  by mapping input data points to means  $\mu(X)$  and variances  $\sigma^2(X)$  of the posterior Gaussian distributions. Then the latent variables  $z$ 's are sampled from this posterior and mapped back into the input space  $\mathcal{X}$ . On the other hand, sampling from the latent distribution  $\mathcal{N}(0, I)$  will facilitate to generate new samples as long as we have trained

the VAE well and obtained a powerful decoder. So examining the quality of the generated samples also serves as an important measure for how well the VAE is trained.

## A. Neural Network Architecture

*a. Datasets* We train on simulated QCD jets collected from fatjet trigger criteria of ATLAS Collaboration.<sup>1</sup> QCD di-jet events are generated with MadGraph [24] for LHC 13 TeV, followed by Pythia8 [25] and Delphes [26] for parton shower and fast detector simulation, respectively. No pile-up was simulated. All jets are clustered using the anti-kt algorithm [27] with cone size  $R = 1.0$  and the selection cut  $p_T > 450$  GeV. Particle flow objects are used for jet clustering, with no jet trimming applied.

*b. Input features and Preprocessing* We take the first 20<sup>2</sup> hardest ( $p_T$  ordered) jet constituents as inputs in the format of four vectors  $\{x_i = (E_i, P_{xi}, P_{yi}, P_{zi}); i = 1, \dots, n\}$  with  $n = 20$ . Jets are preprocessed with minimum transformations to avoid designing effects. Jet constituents are boosted back to the jet rest frame and centered at  $(0, 0)$  in the  $(\eta, \phi)$  plane. Jets are also rotated so that the jet principal axis  $(\sum_i \frac{\eta_i E_i}{R_i}, \sum_i \frac{\phi_i E_i}{R_i})$  (with  $R_i = \sqrt{\eta_i^2 + \phi_i^2}$ ) is vertically aligned on the  $(\eta, \phi)$  plane, with the rotation angle  $\alpha$  indicated in Eq. 3:

$$\tan \alpha = \frac{\sum_i \frac{\phi_i E_i}{R_i}}{\sum_i \frac{\eta_i E_i}{R_i}} \quad (3)$$

*c. VAE Architecture* We explored two simple architectures: Fully Connected Networks (FCN) and Long Short-Term Memory (LSTM) Networks. Since no significant difference in performance was observed, we only present the results for FCN based VAEs (FCN-VAEs) in this work.

For FCN-VAEs, simple dense layers are employed for the encoder and the decoder. ReLU activations are used through latent layers, and linear activation is used in the output layer. The encoder and decoder have symmetric architectures, as the encoder is composed of 256, 128, 64 neurons for each hidden layer. The latent dimension of 10 has been optimized to maximise boosted top signal significance. The Gaussian parameters  $\mu$  and  $\sigma$  are parametrized by dense layers. Then the latent vector  $z$  sampled from the posterior distribution  $\mathcal{N}(\mu, \sigma^2)$

<sup>1</sup> <https://twiki.cern.ch/twiki/bin/view/AtlasPublic/JetTriggerPublicResults>

<sup>2</sup> The number of input jet constituents 20 is chosen to optimize the signal significance of boosted top jets.

is passed to the decoder to reconstruct the output jet. A brief summary of the VAE architecture is depicted in Fig. 3. The reconstruction error is simply chosen as the Mean Squared Error (MSE) between input features  $\{x_i; i = 1 \dots n\}$  and output features  $\{\hat{x}_i; i = 1 \dots n\}$ , as shown in Eq. 4.

$$\mathcal{L}_{\text{VAE}} = \mathcal{L}_{\text{recon}} + \mathcal{L}_{\text{KL}} = \frac{1}{n} \sum_{i=1 \dots n} \|\hat{x}_i - x_i\|^2 + D_{\text{KL}}(q(z|X)||p(z)) \quad (4)$$

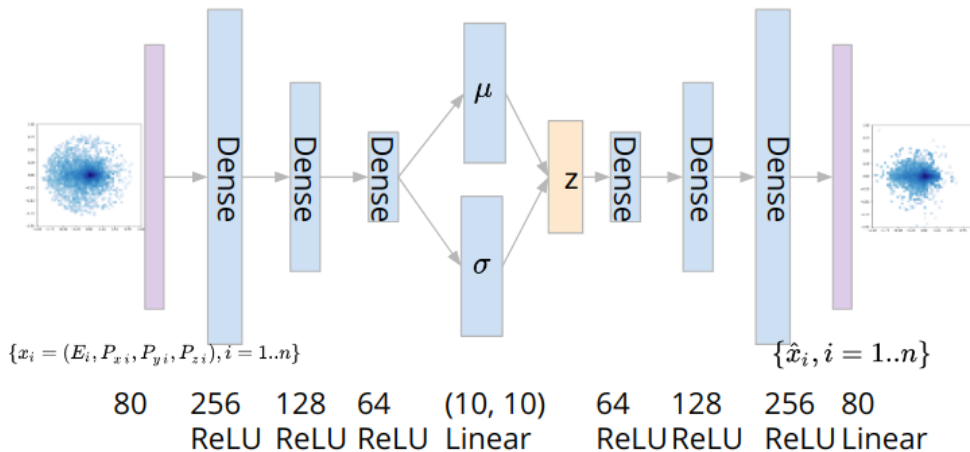


FIG. 3: Architecture of FCN-VAE, with input dimension of 80 and latent dimension of 10. Dense layers with ReLU activations are employed for the encoder and decoder.

## B. Regularization in Latent Space

As introduced previously, KL divergence in the VAE objective can also be viewed as a regularization term. VAEs with variable regularization weight other than 1 are also formulated as  $\beta$ -VAE [28] models. To clarify this process, the empirical objective of a VAE is written as:

$$\mathcal{L}_{\beta\text{-VAE}} = -\mathbb{E}_{z \sim Q}[\log P(X|z)] + \beta D_{\text{KL}}[Q(z|X)||P(z)] = \mathcal{L}_{\text{recon}} + \beta \mathcal{L}_{\text{KL}} , \quad (5)$$

where  $\beta$  is the parameter to denote the relative strength of the latent regularization. Setting  $\beta$  affects the competition between fitting the latent distribution and the input space reconstruction. With  $\beta = 0$  the VAE reduces to the deterministic autoencoder, for which only the reconstruction is optimized during training, resulting in very good jet reconstruction,

however, losing inference capability in the latent space. Increasing  $\beta$  leads to compensation between the jet reconstruction and the latent distribution matching. We have tested different values  $\beta = 0.1, 0.5, 1.0, 5.0$ , and observed that  $\beta = 0.1$  gives better balance between input reconstruction and latent coding. In this paper, we focus on reporting results for  $\beta = 0.1$ .

*a. Training Setup* Throughout this study, we train on 600,000 QCD jets, of which 20% serves as the validation set. We employ Adam [29] algorithm for optimization, with the default values of the parameters. VAEs are trained for 50 epochs with a batch size of 100.

### C. Examining trained VAEs

We examine a few properties of the trained VAE models: jet reconstruction, jet generation, and latent representations.

*a. Jet Reconstruction* To examine how well QCD jets can be reconstructed by VAEs, we show a few distributions of reconstructed high-level jet features in Fig. 4. We see that jet  $p_T$  and mass are both well reconstructed.

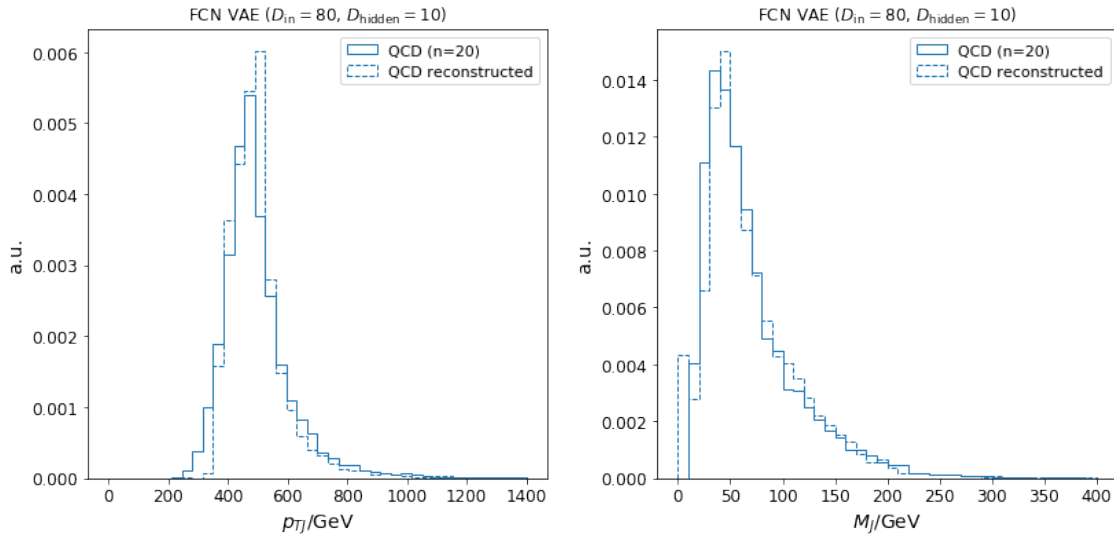


FIG. 4: Reconstructed (*dashed lines*) jet  $p_T$  and  $M_J$ , compared with input jet distributions (*solid lines*) plotted for the first 20 jet constituents with  $p_T$ -ordering.

*b. Jet Generation* To assess the quality of the generative model, we sample from the prior distribution  $\mathcal{N}(0, I)$  in the latent space and generate output jets by passing the sam-

plings through the decoder. We show that the decoded outputs resemble input distributions.

In Fig. 5, we show aggregated distributions of generated features in the input space (after standardization of input features to  $\sim \mathcal{N}(0, I)$ ) and jet images on the  $(\eta, \phi)$  plane. The generated features follow standard Gaussian distributions as we standardized the input features. Generated jet  $p_T$  and  $M_J$  distributions are shown in Fig. 6. Both generated  $p_T$  and  $M_J$  distributions match well with the ones of the original QCD dataset. However, there is a small discrepancy for jet mass, suggesting that the model architecture could be further optimized.

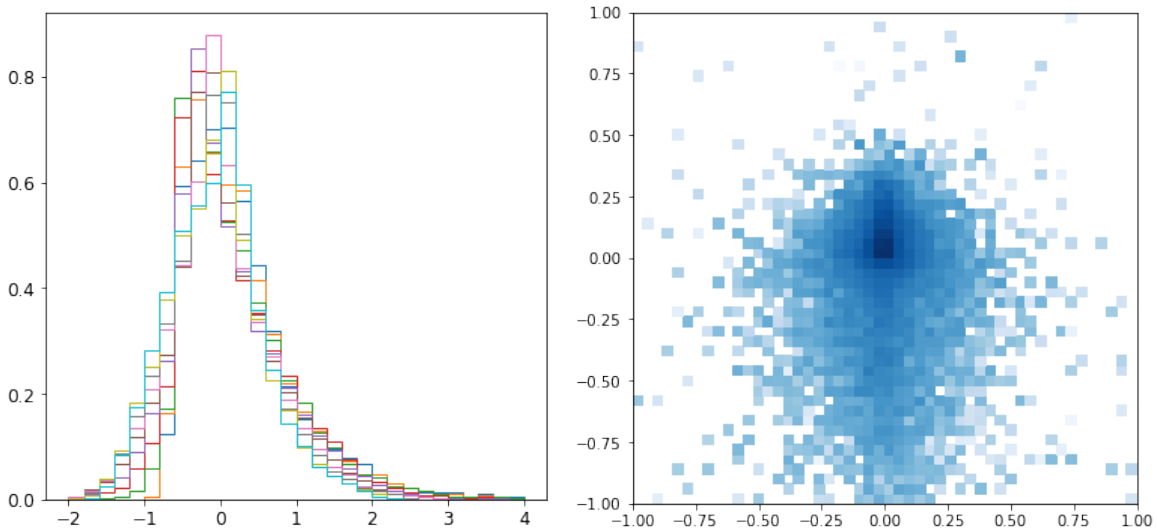


FIG. 5: **Left:** VAE generated input space (scaled) feature distributions. **Right:** VAE generated jet images on the  $(\eta, \phi)$  plane.

*c.  $\beta$ -VAE Latent Representation* As discussed previously,  $\beta$  controls the balance between input reconstruction and latent coding. When  $\beta$  increases, the reconstruction performance might drop since there is extra effort to fit the latent distribution. When  $\beta$  is small, it approaches the behaviour of deterministic autoencoders, in the sense that the regularization strength is weak enough. In Fig. 7, model examination results for  $\beta = 0.1$  are shown. We plot the correlation between reconstruction error and jet mass, the correlation between latent KL divergence and jet mass, the correlation between reconstruction error and latent KL divergence, and the 2d-tSNE [30] (`perplexity = 50`) visualisation for mean values of latent representations for in-distribution QCD jets (**Blue**), out-of-distribution  $W$  jets (**Green**), and out-of-distribution top jets (**Orange**). We observe that the reconstruction error has an

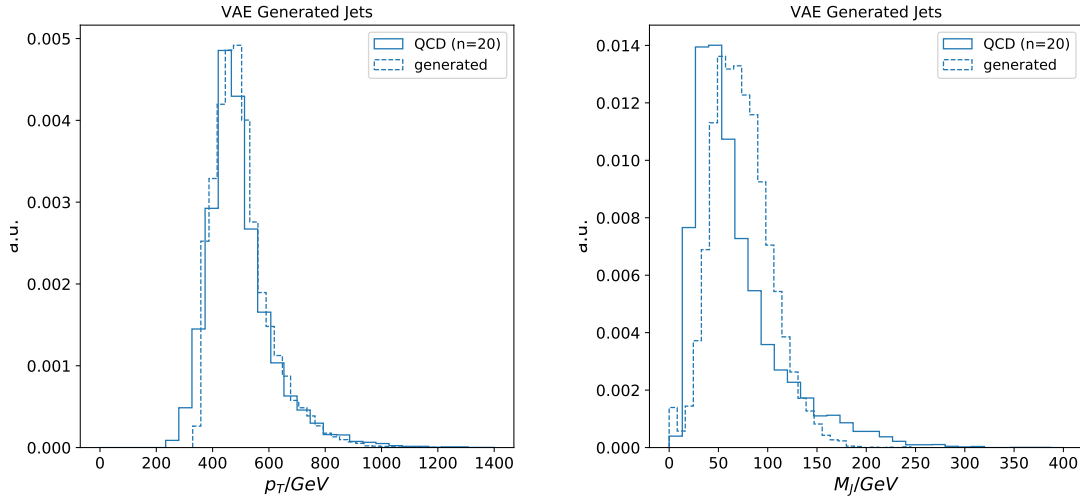


FIG. 6: High-level feature distributions of VAE generated jets (*dashed lines*). **Left:**  $p_T$ ; **Right:**  $M_J$ .

upper-bounded correlation with jet masses. And the latent KL divergence is also (even more strongly and linearly) correlated with jet mass. This suggests that the regularized latent space has encoded relevant information but has different geometry w.r.t. the input space. Little clustering effect is present in 2d-tSNE visualisation. As  $\beta$  increases (see App. A), a stronger clustering effect is observed at the cost that reconstruction is less maintained.

### III. PERFORMANCE IN ANOMALOUS JET TAGGING

In this section, we present the performance of VAE-based anomalous jet taggers, tested on different jet types. Receiver Operating Characteristic (ROC) curves and area under the ROC Curve (AUC) are used for measuring the performance universally.

*a. Test Datasets* A series of test sets [31] are generated to examine the performance of VAE-based anti-QCD jet tagging. Boosted  $W$  jets, top jets, and Higgs jets are generated as representatives of two-prong, three-prong, and four-prong jets. To test jet mass effects, we composed  $W$  jet datasets with rescaled  $W$  jet masses (Standard Model  $W$  jets with only the mass changed for event generation) for comparison. The same mass-rescaling strategy is also applied to top jets. We employ Two Higgs Doublet Models (THDMs) [32] for generating boosted Higgs jets. Heavy Higgs bosons are generated in pairs ( $pp \rightarrow HH$ ), with the

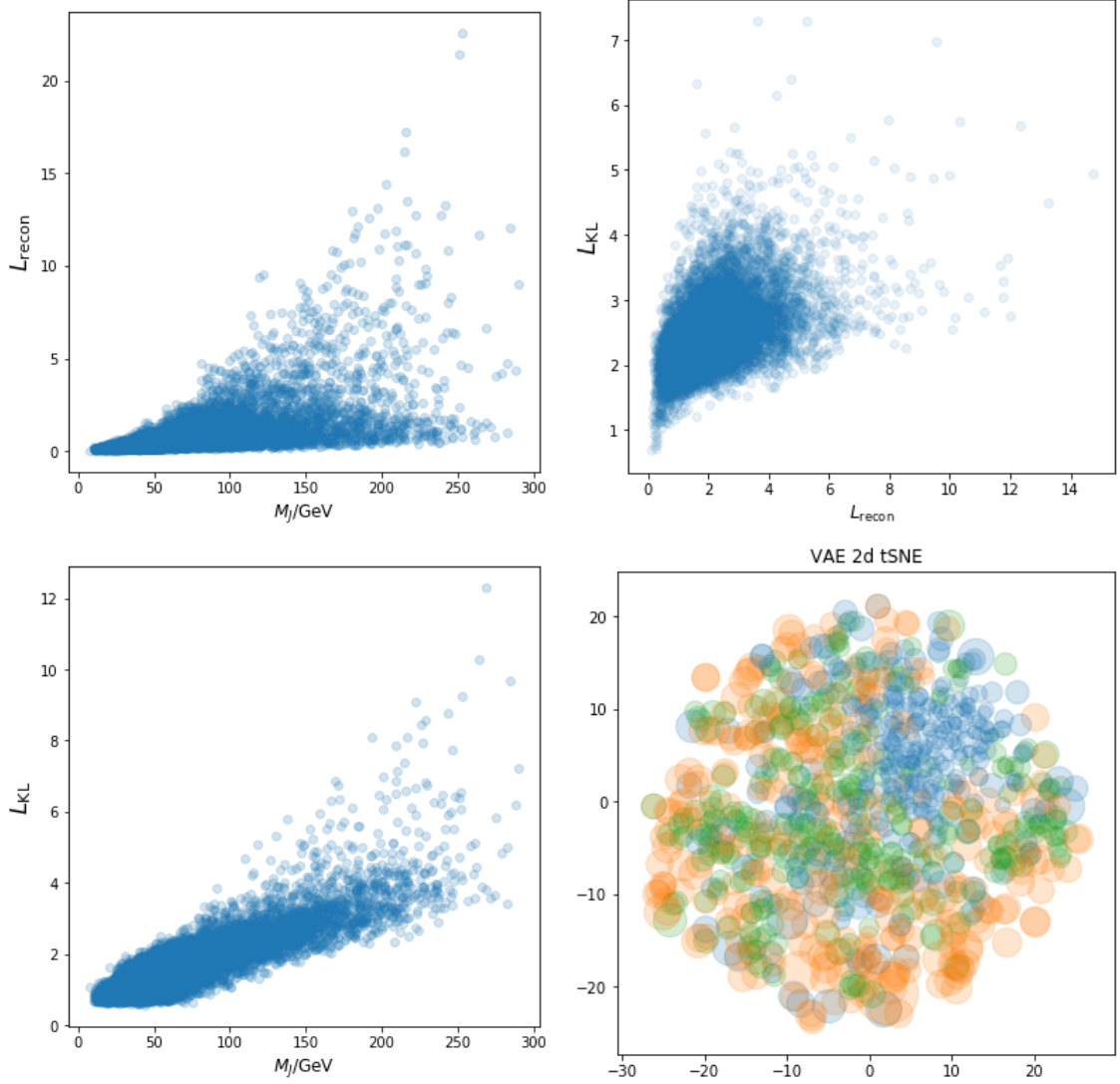


FIG. 7: **Upper-Left:** Reconstruction error v.s. jet mass; **Upper-Right:** KL divergence v.s. reconstruction error; **Lower-Left:** KL divergence v.s. jet mass; **Lower-Right:** Latent 2d-tSNE for different jet types (QCD jets (Blue), W jets (Green) and top jets (Orange)). All plots are for FCN-VAE with  $\beta = 0.1$ .

requirement of jet  $p_T > 450$  GeV and decaying into light Higgs pairs. The light Higgs bosons are then restricted to the  $h \rightarrow b\bar{b}$  decay mode. Different light Higgs masses are experimented to show different degrees of “four-prongness”. With a very light  $m_h$ , boosted heavy Higgs jets will resemble two-pronged jets more. All jets are again clustered using anti-kt algorithm with cone size of  $R = 1.0$ . When testing on these datasets, jet  $p_T$ s are restricted to  $[550, 650]$  GeV for a fair comparison. The test set size for each jet category is

set to be 20,000.

Here is the detailed information for test sets:

- *Two-prong* boosted  $W$  jets are produced by the decay of a heavy resonance  $W'$  with  $m_{W'} = 1.2$  TeV, with  $W$  decaying to light quark jets and  $Z$  decaying to neutrinos:  $pp \rightarrow W' \rightarrow W(jj)Z(\nu\nu)$ . Masses experimented include  $m_W = 59, 80, 120, 174$  GeV.
- *Three-prong* boosted top jets are generated with the decay of a heavy resonance  $Z'$  of  $m_{Z'} = 1.3$  TeV:  $pp \rightarrow Z' \rightarrow t\bar{t}$ . “Top” masses are set to be  $m_t = 80, 174$  GeV. (for  $m_t = 80$  GeV, the decay product  $W$  mass is set to be 20 GeV).
- *Four-prong* boosted heavy Higgs pair production in THDMs is borrowed to generate four-prong samples:  $pp \rightarrow HH$ , with  $H \rightarrow h(bb)h(bb)$  and  $m_H = 174$  GeV,  $m_h = 20, 80$  GeV. In the event generation, we employ  $h_3$  in THDM as the heavy Higgs, and  $h_1$  as the light Higgs.

### A. Anomaly Metric

After successfully training of the VAEs, utilizing the trained models as anomalous jet taggers also requires a good anomaly metric well-defined and specifically tailored.

Even though being the most widely used anomaly metric in the literature, the naive MSE based anomaly metric is confronted with a few problems: there is some correlation with jet constituent numbers, although in fixed input length this effect would be eliminated somehow; and strong mass correlation is generally present. Such effects might be better controlled using an anomaly metric based on the low-dimensional latent representations since the data geometry is expected to be much simpler in that space. We thus explored how the KL divergence from prior to posterior distribution in the latent space works as an anomaly metric. Other than that, the negative log-likelihood (NLL) is also directly considered as an anomaly score.

Independently from the VAE setting, an optimal transport based metric [33] measuring similarities between input jets and reconstructed jets is also tested as an anomaly score. Besides these machine learning based metrics, we found that a simply defined Gaussian model for low-level input features already works well, given proper preprocessing and standardization.

Here is a summary of the options investigated as anomaly metrics:

- Negative log-likelihood:  $\mathcal{L}_{\text{VAE}} = \mathcal{L}_{\text{recon}} + \mathcal{L}_{\text{KL}}$ .
- MSE reconstruction error in input space:  $\mathcal{L}_{\text{recon}} = \frac{1}{n} \sum_i \|\hat{x}_i - x_i\|^2$ .
- KL divergence in latent space:  $\mathcal{L}_{\text{KL}} = D_{\text{KL}}(q(z|x)||p(z))$ .
- Energy Mover’s Distance (EMD): EMD is defined as a metric in the collider space using optimal transport to find the minimum energy moving strategy between two LHC events. The EMD between event  $\mathcal{E}$  and  $\mathcal{E}'$  is defined as:

$$\text{EMD}(\mathcal{E}, \mathcal{E}') = \min_{f_{ij}} \sum_{ij} f_{ij} \frac{\theta_{ij}}{R} + \left| \sum_i E_i - \sum_j E'_j \right|, \quad (6)$$

$$f_{ij} \geq 0, \sum_j f_{ij} \leq E_i, \sum_i f_{ij} \leq E'_j, \sum_{ij} f_{ij} = E_{\min},$$

where  $\theta_{ij}$  is the angular distance between particles indexed with  $i$  and  $j$  in  $\mathcal{E}$  and  $\mathcal{E}'$ , and  $f_{ij}$  denotes the energy being moved between events.  $E_{\min} = \min\{\sum_i E_i, \sum_j E'_j\}$ .  $R$  is a weight parameter and is set to be 1.0 in our practice. We calculate EMDs between input jets and output jets as the anomaly score. We thus expect out-of-distribution jets will give larger EMDs in the sense that they will not be easily reconstructed. We have already normalized jet  $p_{\text{T}}$ s to eliminate the contribution from pure energy difference in the second term of Eq. 6.

- MSS: simple mean squared sum (MSS) after standardizing input features to follow  $\sim \mathcal{N}(0, I)$ :  $\frac{1}{n} \sum_i \|x_i\|^2$ . This can be seen as the simple  $\chi^2$  of standardized input features.

## B. Results

We first present the ROC curves for NLL based anomaly score. This is aiming at seeing the general responses on different jet types. In Fig. 8, ROC curves under NLL are presented for different test jet types.

From the plot, it’s obvious that the VAE performance in the value of AUC is correlated with jet mass. For mass-rescaled  $W$  jets and top jets, they all show the same trend. As for the jet complexity, we take the jet mass of 174 GeV as a benchmark (red lines). We observe

that top jets have the highest discriminative scores, while  $W$  and Higgs jets have slightly lower AUCs.<sup>3</sup> In the rest frame of the heavy Higgs, light Higgs jets with very small mass are almost produced back to back and are very boosted. Thus  $h3$  with decaying product  $h1$  of a mass of 20 GeV should behave similarly to two-prong jets. In Fig. 8,  $h3(h1=20\text{GeV})$  has a lower AUC w.r.t.  $h3(h1=80\text{GeV})$ , as expected. As a quick conclusion, there is limited yet manifested correlation with jet “complexity”.

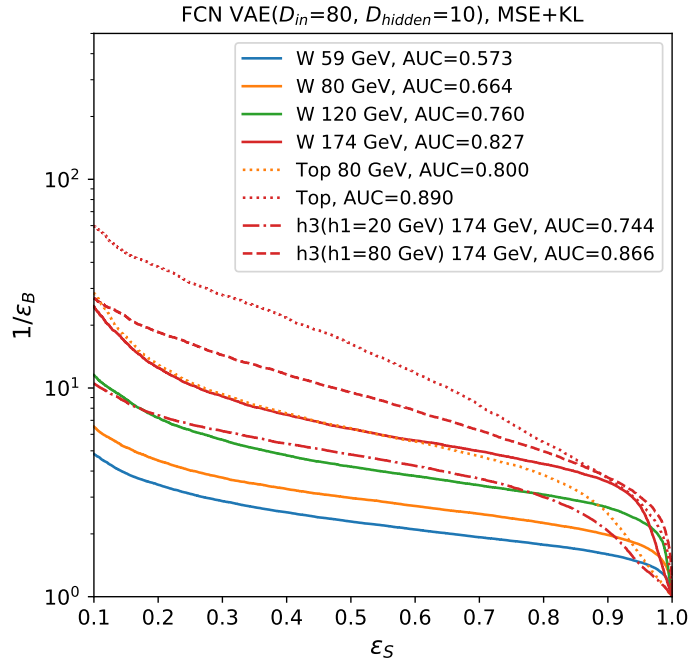


FIG. 8: ROC curves for different jet types, with NLL as the anomaly score. Colors are used to denote jet masses, while different line styles are used for different jet types. We have solid lines for  $W$  jets, and red indicates the benchmark mass of 174 GeV for any jet type.

Then we focus on examining different anomaly metrics. In Fig. 9, we show results for the other anomaly metrics introduced previously. From the AUC numbers, they have very similar discriminative power, in the sense that there is no significantly better or worse numbers present. And the mass correlation trend holds for all metrics. Respectively speaking, MSE and EMD performs most similarly. This makes sense since they both measure the similarity in input space. Especially for KL and MSS, the differences coming from jet types are reduced

<sup>3</sup> This might be because we tuned a few hyper-parameters according to the top test set.

w.r.t. the other two metrics, while the mass correlation effect is even more obvious. As shown in last section, the KL divergence is strongly correlated with the jet mass, which coincides with this observation. In real applications, one will need to choose an adapted anomaly score according to the specific problem at hand.

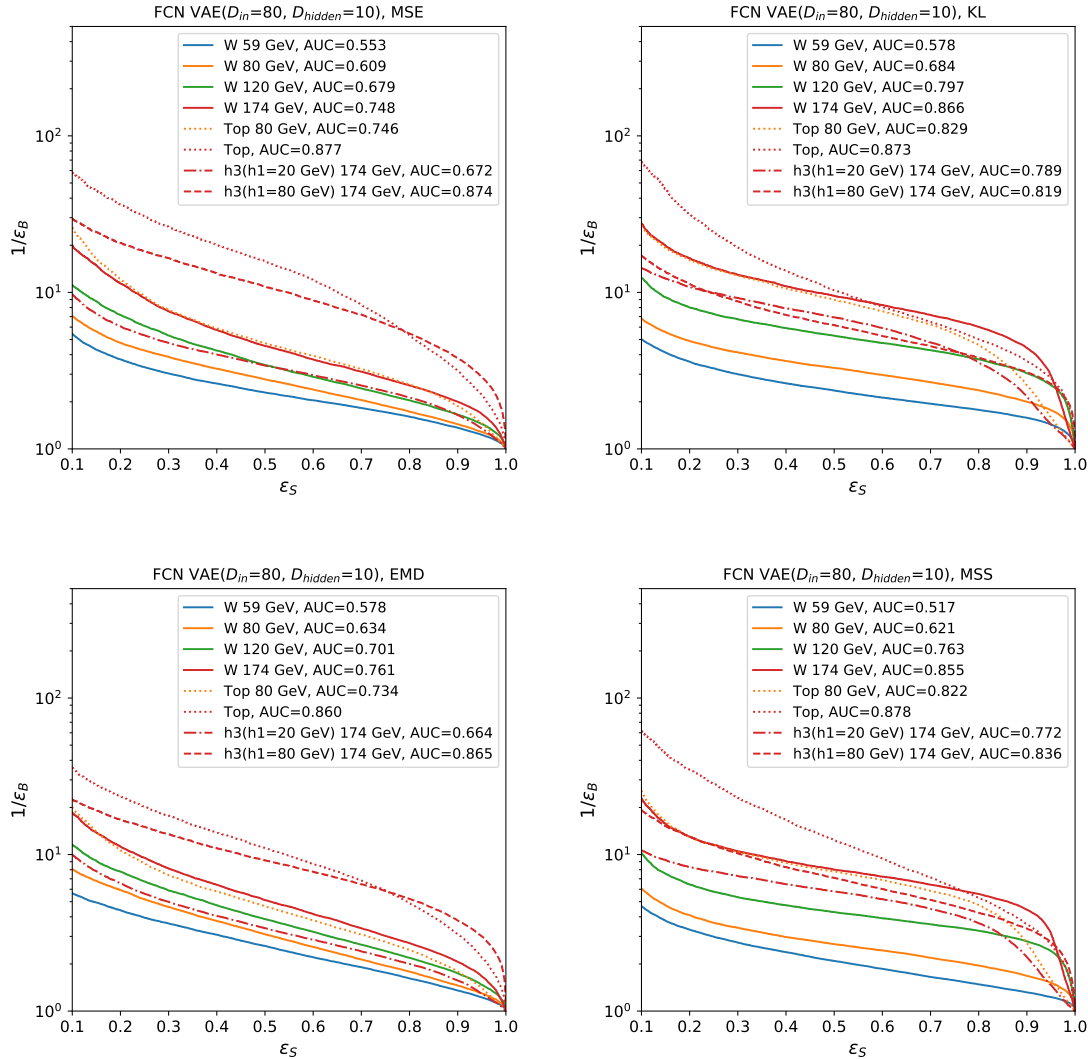


FIG. 9: ROC curves for different jet types, with anomaly metric of MSE reconstruction error (*Upper-left*), KL divergence (*Upper-right*), EMD (*Lower-left*) and MSS (*Lower-right*), respectively.

Since the mass correlation is obvious, low-mass jets generally give low AUCs. This brings difficulties in tagging jets with lower masses. For instance,  $W$  jets with a mass of 80 GeV can only reach the  $AUC \sim 0.68$  in the best case. We will see how this can be amended in later sections.

#### IV. MASS DECORRELATION

As mentioned in previous sections, MSE-based autoencoders, be it built with four vectors or in the format of images, are highly correlated with jet mass, when tagging anti-QCD anomalies. In Fig. 10, we show the mass-sculpting effects of reconstruction error based tagger. Higher reconstruction error selects a sample of high-mass QCD jets.

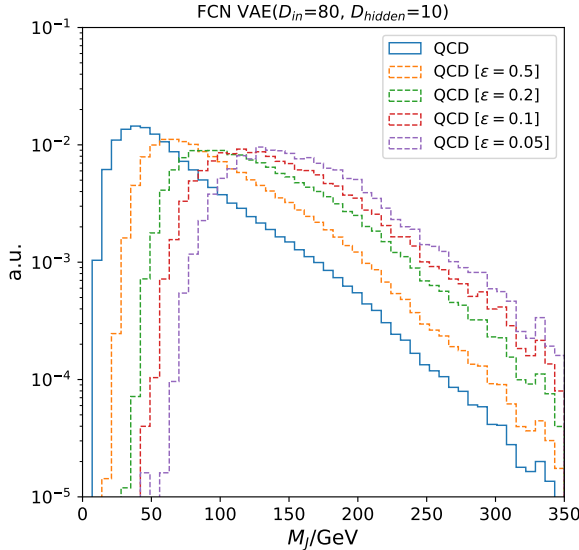


FIG. 10: QCD background mass distributions after thresholding VAE reconstruction errors at different background efficiencies  $\epsilon$ .

Mass decorrelation is thus an important topic in general search for resonances using large-radius jets. For example, the bump-hunting analysis utilizes orthogonal information w.r.t. jet mass to reduce the background and then carries out a bump search in the mass dimension. So we dedicated a study to mass-decorrelated taggers in this section. Previous works have utilized adversarial training to decorrelate jet mass for either classifiers [21, 22, 34, 35] or autoencoders [12]. However, adversarial training is difficult to tune and takes much more computational resources. We instead employ the distance correlation (DisCo) regularization [20] as a mass-decorrelation baseline.

*a. DisCo-VAE* In the DisCo approach, a distance correlation regularization term is added to the VAE loss as indicated in Eq. 7:

$$\mathcal{L}_{\text{DisCo-VAE}} = \mathcal{L}_{\beta\text{-VAE}} + \kappa R_{\text{DisCo}}, \quad (7)$$

where the regularizer  $R_{\text{DisCo}}$  is defined in Eq. 8 as the distance correlation between the VAE loss and the jet mass.

$$R_{\text{DisCo}} = \text{dCor}(M_J, \mathcal{L}_{\beta\text{-VAE}}). \quad (8)$$

Distance correlation [36] is a measure of the non-linear correlation between two variables. Independent variables will give a distance correlation of 0. The distance correlation  $\text{dCor}(X, Y)$  between variable  $X$  and  $Y$  is defined as in Eq. 9, with the distance covariance  $\text{dCov}(X, Y)$  defined in Eq. 10, where  $(X', Y')$  and  $(X'', Y'')$  are independent and identically distributed samples of  $(X, Y)$ .  $\text{dVar}(X)$  and  $\text{dVar}(Y)$  are simply the distance variances defined by  $\text{dVar}(\cdot) = \text{dCov}(\cdot, \cdot)$ . And  $\text{cov}(\cdot, \cdot)$  denotes the classical Pearson covariance.

$$\text{dCor}(X, Y) = \frac{\text{dCov}(X, Y)}{\sqrt{\text{dVar}(X)\text{dVar}(Y)}} \quad (9)$$

$$\begin{aligned} \text{dCov}^2(X, Y) &= \langle \|X - X'\| \|Y - Y'\| \rangle + \langle \|X - X''\| \|Y - Y''\| \rangle - 2\langle \|X - X'\| \|Y - Y''\| \rangle \\ &= \text{cov}(\|X - X'\|, \|Y - Y'\|) - 2\text{cov}(\|X - X'\|, \|Y - Y''\|) \end{aligned} \quad (10)$$

For DisCo-VAE, we tested different  $\kappa$  values ( $\kappa = 0.1, 0.5, 1, 10, 100, 200, 500, 1000$ )<sup>4</sup>, and found that  $\kappa = 100$  gives a balanced result for our VAE model, in the sense that both mass decorrelation and anomaly detection capability are maintained. We simply employ NLL as the anomaly score here. In Fig. 11, we show mass decorrelation effects for DisCo-VAE with  $\kappa = 100$  and  $\kappa = 1000$  respectively. Although  $\kappa = 1000$  gives very good mass decorrelation, we find that it's not able to preserve good enough anomaly detection capability. In Fig. 12, we present the ROC curves after mass-decorrelation for DisCo-VAEs. For all test sets, poor anomaly detection performance is observed compared to the results presented in Fig. 8 and 9. There are even a few test sets giving AUCs less than  $\sim 0.5$ , which again reminds us of the failure case discussed in the last section.

---

<sup>4</sup> Annealing training is also applied here.

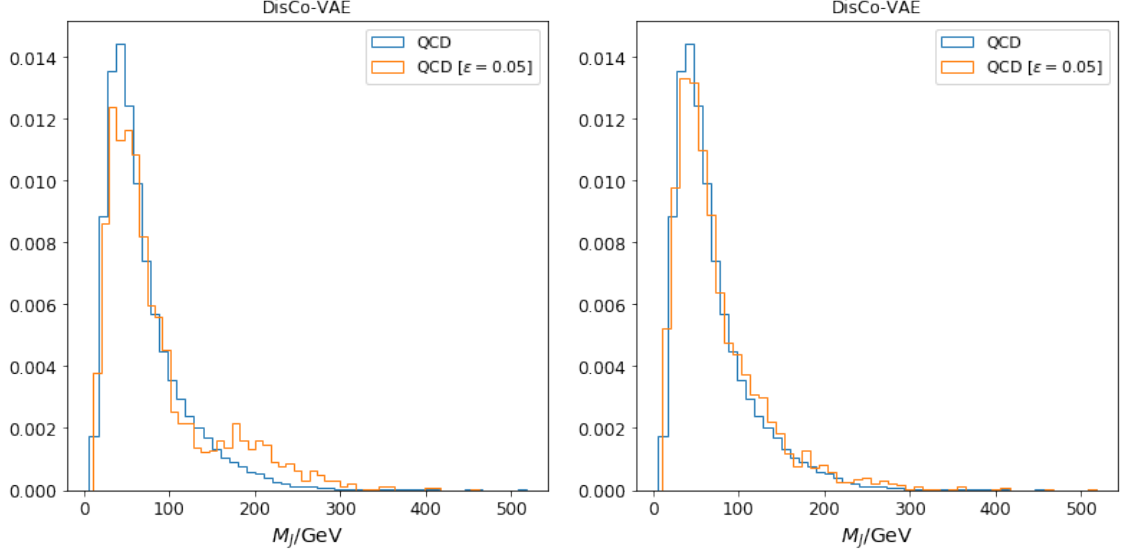


FIG. 11: Mass decorrelation effects for DisCo-VAEs with  $\kappa = 100$  (*Left*) and  $\kappa = 1000$  (*Right*).

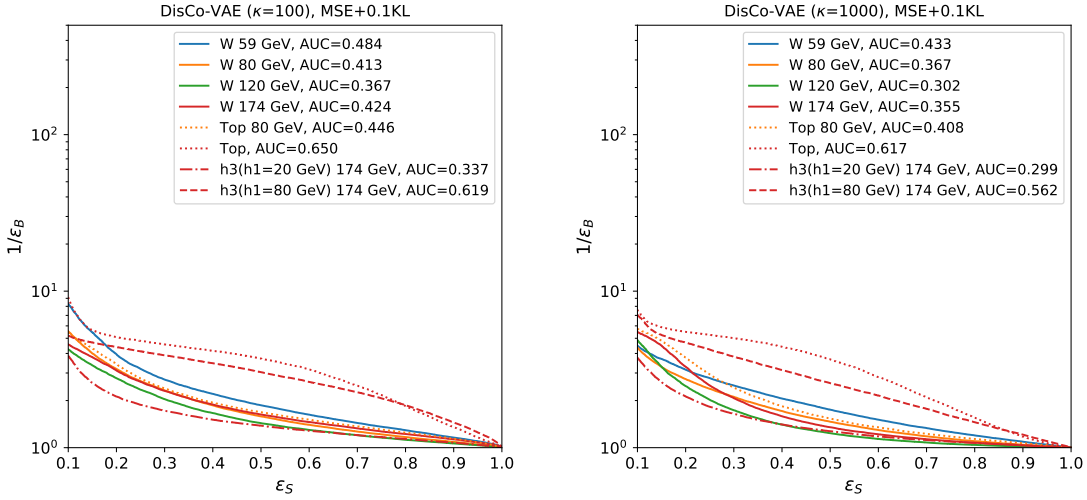


FIG. 12: ROC curves for DisCo-VAE with  $\kappa = 100$  (*Left*) and  $\kappa = 1000$  (*Right*).

## V. SEMI-SUPERVISION – OE-VAE

Based on the observations presented in previous sections, the current situation is that the mass-correlation is strong for simple VAEs while the mass-decorrelated DisCo-VAE taggers have poor discrimination performance in the full test spectrum. There are cases that OoD samples are even assigned higher probability than InD samples. This calls for novel approaches to the problem under investigation. When unsupervised learning might find bad

minima for which not much discriminating power is enabled, semi-supervised learning may help with this situation. One approach which might help with gaining higher sensitivity in anomaly detection is the Outlier Exposure (OE) [19]. By injecting some OoD samples in the training process and requiring the model to detect the exposed OoD samples, the VAEs will learn problem-oriented heuristics to help detect general OoD anomalies. This Outlier Exposed VAE (OE-VAE) is similar to training an auxiliary-classifier, in a pseudo-binary manner for which inliers and outliers are required to be separable.

In the tailored OE-VAE approach, we try to achieve two goals at the same time: increasing sensitivity to out-of-distribution samples, and decorrelating jet mass from the anomaly score. By simply exposing outliers to the VAE training, we hope to obtain a general sensitivity increase by this auxiliary task, not only to the exposed samples but also generalized to other types of anomalies. Another advantage of having an outlier dataset is that we thus have a handle to provide extra guidelines for our training tasks. A simple and useful practice is that we match the mass distribution of inlier samples and outlier samples to successfully decorrelate the jet mass. This is a very simple yet powerful trick under the current problem setting.

We employ mass-rescaled boosted  $W$  jet samples as outliers exposed to the VAE training process. As mentioned in Section III, a spectrum of boosted  $W$  jets are produced by rescaling Standard Model  $W$  mass and generated with the process  $pp \rightarrow W' \rightarrow W(jj)Z(\nu\nu)$ . We resampled the mixture of these mass-rescaled  $W$  jets to match their mass distribution to that of the QCD samples. This procedure is similar to the classical approach “planning” [21] in principle. One may of course use other modern techniques to decorrelate mass. However, in the setting of Outlier Exposure, it comes natural to take advantage of the outlier dataset.

The learning objective of OE can be written as adding a penalty term contributed from outliers  $x'$  to the original VAE loss term, as in Eq. 11:

$$\mathbb{E}_{(x \sim D_{InD})} \mathcal{L}_{\beta\text{-VAE}}(x) + \lambda \mathbb{E}_{(x \sim D_{InD}, x' \sim D_{OoD})} \mathcal{L}_{\text{OE}}(x, x'), \quad (11)$$

where  $\lambda$  controls the relative strength of OE. The OE loss term  $\mathcal{L}_{\text{OE}}$  gains its concrete form according to tasks at hand.

For convenience, we rewrite the OE-VAE loss function as  $\mathcal{L}_{\text{OE-VAE}} = \mathcal{L}_{\beta\text{-VAE}} - \lambda \mathcal{L}_{\text{OE}}$ . The outlier exposure can be performed either in input space or in latent space. In the following we discuss both cases.

- MSE-OE: in the input space, the OE loss can be written in the sigmoid activation of the difference between mean squared reconstruction error of InD samples and OoD samples. This is very similar to an auxiliary task of classification between InD and OoD:

$$\mathcal{L}_{\text{OE}} = \sigma_{\text{sigmoid}}(\text{MSE}_{\text{OoD}}(x', \hat{x}') - \text{MSE}_{\text{InD}}(x, \hat{x})) \quad (12)$$

- KL-OE: we assume that the geometry would be flattened and more linearized in the latent space. It is thus reasonable to employ the margin loss as follows:

$$\mathcal{L}_{\text{OE}} = \min\{0, \mathcal{L}_{\text{KL, OoD}}(z') - \mathcal{L}_{\text{KL, InD}}(z) - \text{margin}\}, \quad (13)$$

with  $z'$  denoting latent representation of outlier samples. This will encourage outlier samples to have a larger KL loss above a specific margin.

Of course these are not unique choices for the OE loss. But they have been effective in our studies.

*a. Training Setup* We exposed 120,000 OoD samples consisting of boosted (mass-rescaled)  $W$  jets, which are resampled to match the mass distribution of the QCD background. Increasing  $\lambda$  puts higher weight on the supervision part and, at the same time, enforces stronger mass-decorrelation. Thus  $\lambda = 500$  was chosen for MSE-OE accordingly to make sure both the VAE loss and the OE penalty are equally optimized. For KL-OE, we have  $\lambda = 2$  and `margin` set to 1 according to mean values of the KL divergence. We cyclically anneal  $\lambda$ <sup>5</sup> in the training process to achieve a better balance between the optimization of the VAE loss and the OE loss. The OE training can be carried out either from scratch or in the manner of fine-tuning a pre-trained VAE model. We report results for the models that were trained from scratch in the following.

*b. Results* In Fig. 13, we present ROC curves for different jet types after OE training for MSE-OE and KL-OE respectively. The left panel shows ROC curves for MSE-OE. We accordingly employ mean squared reconstruction error as the anomaly score. The first observation is that the  $W$  tagging performance is immediately improved. Respectively, a few test sets such as top have lower AUCs compared to Fig. 8 and 9. This is mainly

---

<sup>5</sup> Slowly increase  $\lambda$  from 0 to the target value for multiple times.

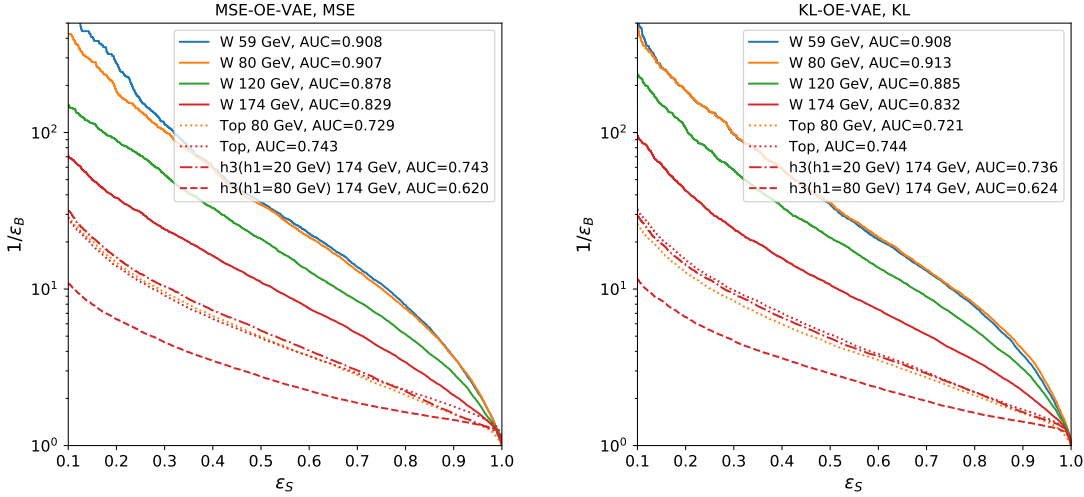


FIG. 13: **Left:** ROC curves for MSE-OE VAE ( $\lambda = 500$ ); **Right:** ROC curves for KL-OE VAE ( $\lambda = 2$ ,  $\text{margin} = 1$ ).

due to the extra mass-decorrelation. This point can be further justified from comparison with the results of DisCo-VAE, for which only mass-decorrelation effects was introduced. Mass-decorrelation generally drops the AUCs of high mass jets. In comparison, the semi-supervision gains more discrimination for top jets. The right panel of Fig. 13 presents ROC curves for KL-OE, for which the KL divergence in latent space is the anomaly score. Generally speaking, the performance is very similar to MSE-OE.

We then examined mass decorrelation effects for OE-VAEs. The results are shown in Fig. 14 for MSE-OE and KL-OE respectively. Excellent mass decorrelation effects are achieved in both scenarios. One thing to keep in mind is that only outlier exposed metrics can be used for mass-decorrelated taggers. For instance, MSE-OE-VAE paired with KL-based anomaly detection will not effectively achieve mass decorrelation. The equivalent “planning” effects only affects one space: the input space or the latent space. Thus one should match the anomaly metric with the OE training scenario, i.e., if one trains OE in the input space, then accordingly using input space MSE anomaly metric will provide the desired mass decorrelation.

This is not a full account of the application of Outlier Exposure, or more broadly semi-supervised learning, in generative model based anomalous jet tagging. We have shown that the naive generative model, in our current settings (training dataset, encoding architecture,

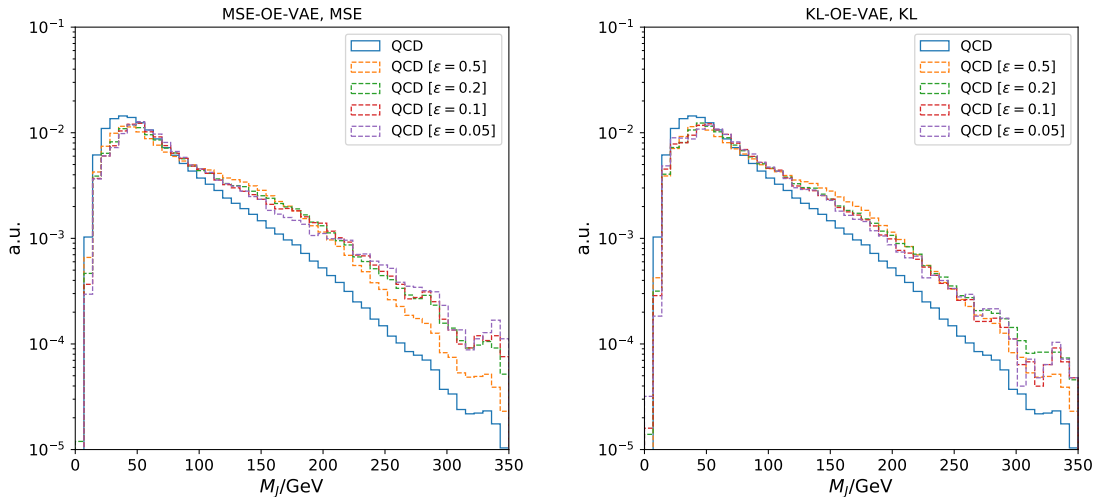


FIG. 14: Mass decorrelation effects in MSE-OE (*Left*) and KL-OE (*Right*).

generative modeling), is not enough to bring a powerful generic anomalous jet tagger. It’s encouraging to see possible solutions to enhance the tagger’s performance.

*c. DisCo-VAE v.s. OE-VAE* To see more clearly how much performance can be achieved by OE-VAEs, we compare with DisCo-OE which is also mass-decorrelated. To make a more quantitative examination of the mass-decorrelation quality, we employ the measure based on Jensen-Shannon Divergence (JSD, Eq. 14), which is the symmetric version of KL Divergence to measure the similarity between two probability distributions. Generally speaking, the lower JSD is, the better two distributions match. So for an anomalous jet tagger, we expect a low JSD, and at the same time a high AUC.

$$D_{\text{JS}}(p(m)||p'(m)) = \frac{1}{2}(D_{\text{KL}}(p(m)||\bar{p}(m)) + D_{\text{KL}}(\bar{p}(m)||p(m))), \quad \bar{p}(m) = \frac{p(m) + p'(m)}{2} \quad (14)$$

In Fig. 15. We plot inverse JSD w.r.t. signal efficiency at background efficiency 5% for the top test set. OE-VAEs generally have much higher signal efficiency w.r.t. DisCo-VAEs at the same mass-decorrelation level. It’s promising that OE-VAEs retain very good anomaly detection power while at the same time being mass-decorrelated.

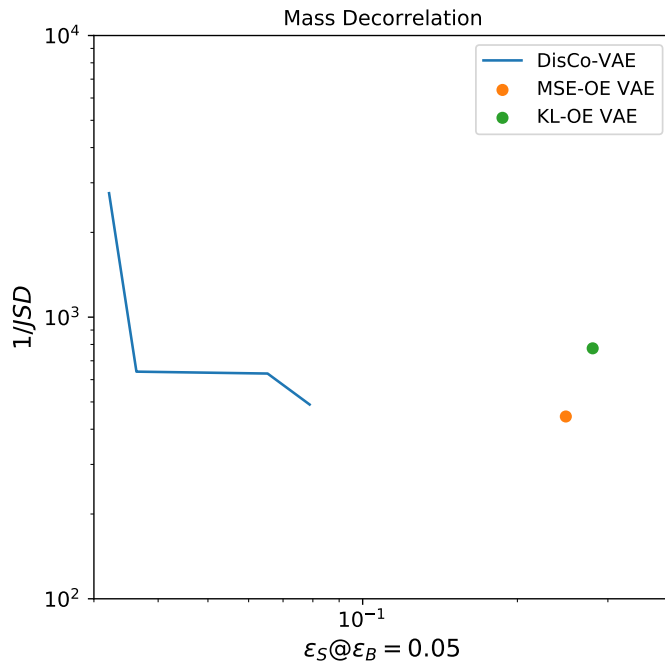


FIG. 15: Jensen-Shannon Divergence v.s. Signal Efficiency for mass-decorrelated VAEs. Different  $\kappa$  values ( $\kappa = 100, 200, 500, 1000$ ) are shown for DisCo-VAE.

## VI. SUMMARY AND DISCUSSIONS

Unsupervised learning is a promising approach for model-independent new physics searches at the LHC. We carefully investigated Variational Autoencoders for anti-QCD anomalous jet tagging, totally based on low-level input features. To better regularize the latent space and achieve a good balance between jet reconstruction and latent space inference, we cast this work in a generalized VAE setting –  $\beta$ -VAE, for which the latent KL divergence is placed with a variable weight. We examined the VAE properties, including reconstruction performance, generation ability, and latent representations, of the trained VAEs. High-level features such as jet  $p_T$  and jet mass are correctly reconstructed, and the generative model also performs very well.

To systematically assess the anomalous jet tagging performance, we generated a comprehensive series of test sets including mass-rescaled  $W$  jets, top jets, and Higgs jets, as representatives of jet “prongness”. Different anomaly metrics were studied. A strong mass correlation is generally observed for all the anomaly scores studied, leading to smaller and

unsatisfying AUCs for low-mass jets.

As an important application of anti-QCD jet taggers, jet based heavy resonance searches benefit from a mass-decorrelated tagger which makes background estimation accessible. Aiming at a mass-decorrelated tagger, we employed the distance correlation method, using the distance correlation between jet mass and VAE objective as a regularizer. While eliminating mass sculpting effects, the general performance in anti-QCD tagging has been found to be not very practical.

To achieve higher sensitivity to out-of-distribution samples and at the same time decorrelate the jet mass from the anomaly score, we employed the Outlier Exposure technique to help learn more effective latent representations. By injecting some outlier samples to the VAE training process in the manner of auxiliary tasks, sensitivity to outliers is generally increased. By matching the outlier mass distribution to the inlier QCD mass distribution, we achieved very good mass-decorrelation at the same time. OE-VAEs are compared to the baseline DisCo-VAEs in a two-dimensional measure of the ability of decorrelating jet mass and detecting anomalies. OE-VAEs are generally gaining much better performance. We found that Outlier Exposure is a very simple yet effective trick to improve the performance of deep generative models, specifically VAEs in this work, in the scope of anomalous jet tagging.

In this work, we formulate the problem of using generative models (specifically Variational Autoencoders) to detect out-of-distribution samples in jet physics for the LHC. Assisted with a comprehensive testing system, we observe that unsupervised learning without any guidelines might not give the optimal solution for specific tasks. A simple semi-supervised approach to enhance the performance and mitigate potential deployment failures is investigated. Despite this effort, there are still several improvements that could be pursued. In this study, only a simple encoding architecture of FCN is used. An LSTM model is also investigated, but not much effort is spent on exploring more complex encoding architectures. We expect improved reconstruction ability in that case. In the standard VAE, latent priors are simply multivariate Gaussian distributions. This can be extended to more complex latent priors. Besides these, alternative reconstruction error formats or input space similarity metrics can be explored to better represent the input space structure. We leave these possibilities to the future work.

## Acknowledgments

This work is supported by IVADO Fundamental Research Grant and Natural Sciences and Engineering Research Council of Canada (NSERC). The authors would like to acknowledge Amir Farbin, Debottam Bakshi Gupta, Takuya Nobe, and Johnny Raine for early participation in the project. TC would like to thank Faruk Ahmed, Aaron Courville and Florian Bordes for helpful discussions on anomaly detection in the general machine learning community.

## Appendix A: Regularization Strength Affects VAEs' Behaviour

As discussed in Sec. II, the regularization strength  $\beta$  will affect the optimization of jet reconstruction and also the latent distribution. In Fig. 16, reconstructed jet observables are shown for different  $\beta = 0.1, 0.5, 1.0$ . When  $\beta$  increases, reconstruction performance drops. In Fig. 17, tSNE visualisation of latent representations is shown. As  $\beta$  increases, in the latent space there is clustering effect emerging.

## Appendix B: Supervised $W/QCD$ Classifier v.s. OE-VAE

Since we utilized an extra  $W$  jet dataset in the semi-supervision approach, it will be interesting to see how the results are compared with supervised  $W/QCD$  DNN classifiers. We employ a fully-connected DNN architecture ( $\text{ReLu}(256) \rightarrow \text{ReLu}(128) \rightarrow \text{ReLu}(64) \rightarrow \text{ReLu}(6) \rightarrow \text{Sigmoid}$ ), and train with the same datasets and input features as in OE-VAE training<sup>6</sup>. To compare with mass-decorrelated VAE models, we also trained with reweighted samples to decorrelate mass for a supervised  $W/QCD$  tagger. The mass decorrelation results are shown in Fig. 18. ROC curves for both taggers are shown in Fig. 19. In general,  $W/QCD$  classifier tags  $W$  jets with different masses quite efficiently. A mass-decorrelated  $W/QCD$  tagger can also be used to tag other jet types, although with sub-optimal performance. This is due to the remaining transferability of supervised taggers [5, 37].

In Fig. 20, we compare tagging performance on held-out classes (top and Higgs jets) of supervised  $W/QCD$  classifier and VAE models. On the left panel, we compare the  $W/QCD$

---

<sup>6</sup> Class weights are employed to balance dataset size of different classes.

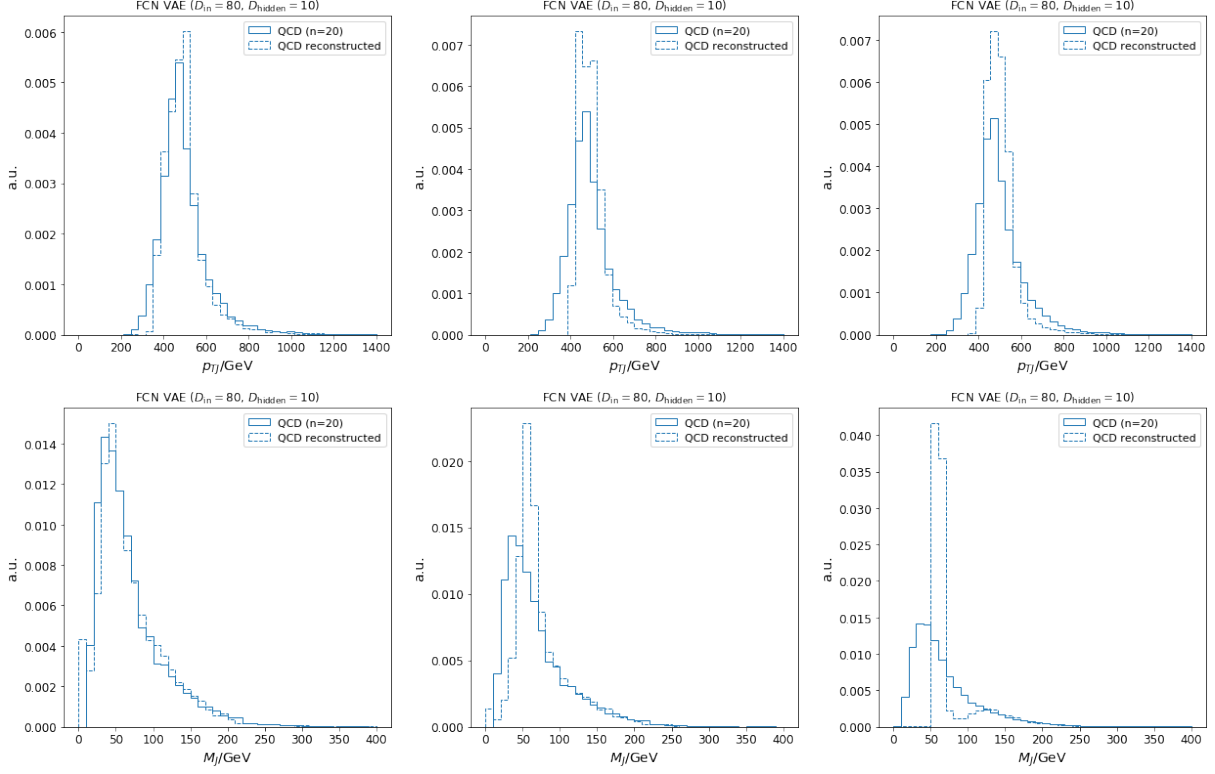


FIG. 16: Reconstructed jet  $p_T$  (*Upper*) and  $M_J$  (*Lower*) for different  $\beta$ 's. **Left:**  $\beta = 0.1$ ; **Middle:**  $\beta = 0.5$ ; **Right:**  $\beta = 1.0$ .

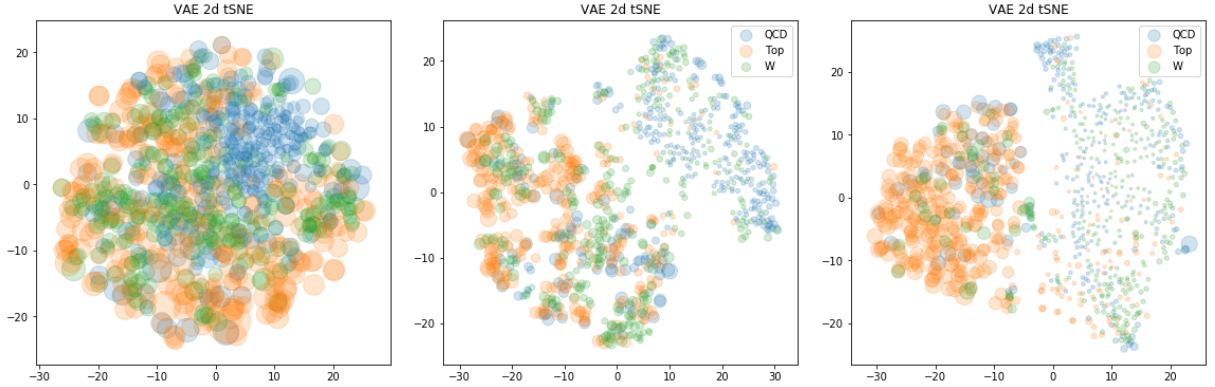


FIG. 17: tSNE visualisation of the latent representations (QCD jets (Blue),  $W$  jets (Green) and top jets (Orange)). **Left:**  $\beta = 0.1$ ; **Middle:**  $\beta = 0.5$ ; **Right:**  $\beta = 1.0$ .

classifier with simple VAE for detecting top jets and Higgs jets. VAE generally has better performance regarding these held-out classes. However, it's not a completely fair comparison, since both taggers are mass-sculpted. For a fair comparison, we thus compare OE-VAEs

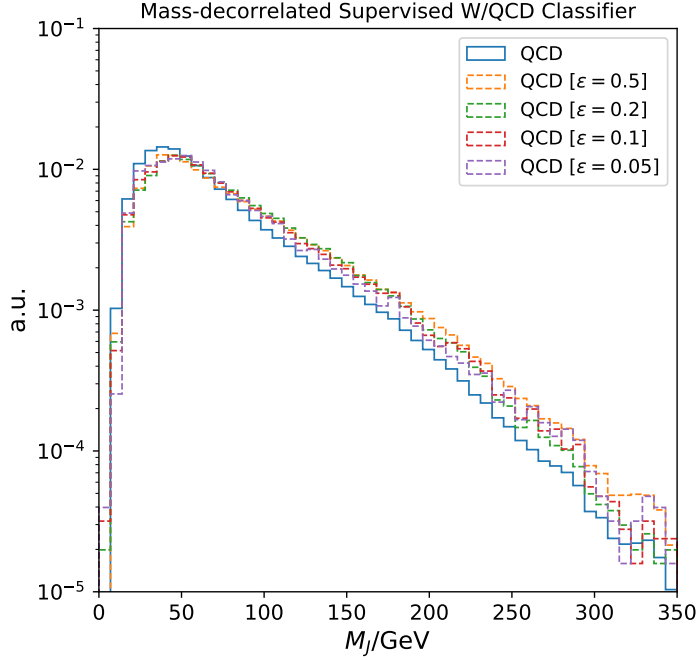


FIG. 18: Mass decorrelation results for the mass-decorrelated supervised  $W/QCD$  classifier.

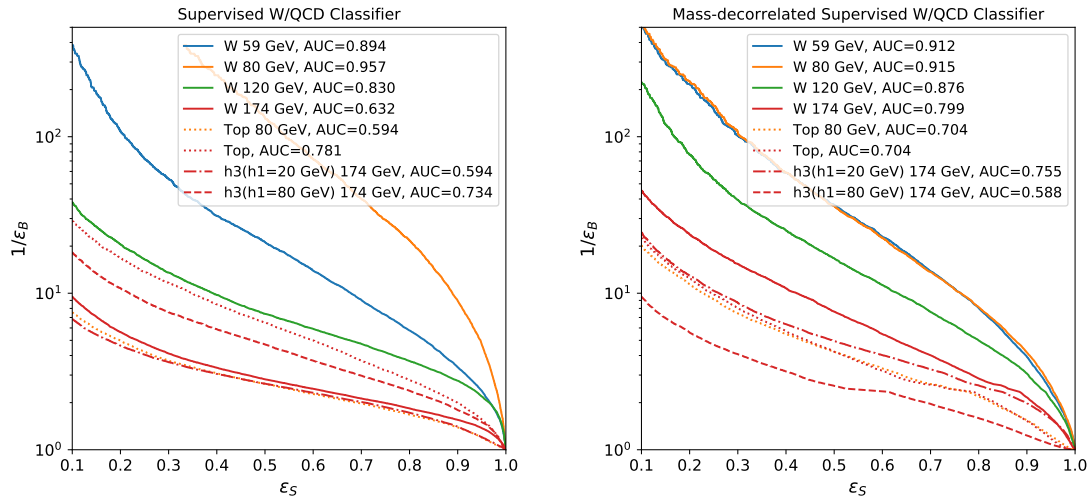


FIG. 19: **Left:** ROC curves for the supervised  $W/QCD$  classifier; **Right:** ROC curves for the mass-decorrelated supervised  $W/QCD$  classifier.

with the mass-decorrelated  $W/QCD$  classifier on the middle and right panels of Fig. 20. On

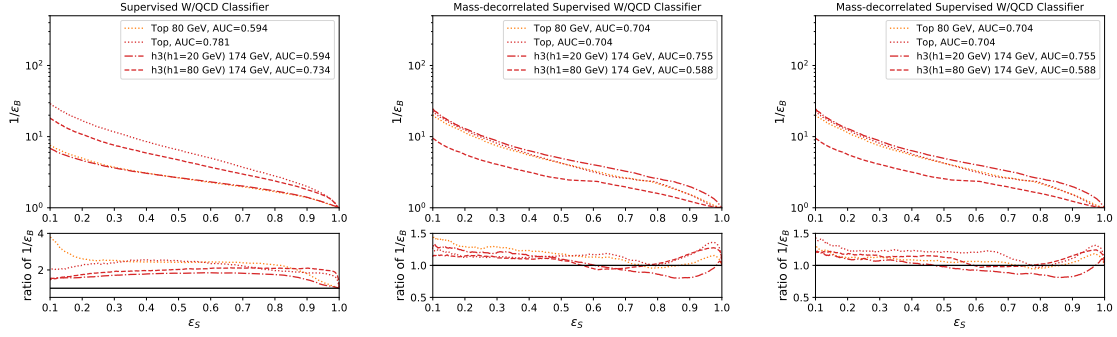


FIG. 20: ROC curves for held-out classes. In the upper part, ROC curves from (mass-decorrelated)  $W/QCD$  classifier are shown, while in the lower part, the ratios of  $1/\epsilon_B$  of (OE-)VAEs to  $W/QCD$  classifier are presented. **Left:** VAE v.s.  $W/QCD$  classifier; **Middle:** MSE-OE v.s. mass-decorrelated  $W/QCD$  classifier; **Right:** KL-OE v.s. mass-decorrelated  $W/QCD$  classifier.

most of the working points of  $\epsilon_S$ , the OE-VAEs outperform the  $W/QCD$  classifier.

- 
- [1] J. H. Collins, K. Howe, and B. Nachman, “Anomaly Detection for Resonant New Physics with Machine Learning,” *Phys. Rev. Lett.* **121** no. 24, (2018) 241803, [arXiv:1805.02664 \[hep-ph\]](#).
  - [2] J. H. Collins, K. Howe, and B. Nachman, “Extending the search for new resonances with machine learning,” *Phys. Rev.* **D99** no. 1, (2019) 014038, [arXiv:1902.02634 \[hep-ph\]](#).
  - [3] J. Hajer, Y.-Y. Li, T. Liu, and H. Wang, “Novelty Detection Meets Collider Physics,” [arXiv:1807.10261 \[hep-ph\]](#).
  - [4] B. Nachman and D. Shih, “Anomaly Detection with Density Estimation,” [arXiv:2001.04990 \[hep-ph\]](#).
  - [5] J. A. Aguilar-Saavedra, J. H. Collins, and R. K. Mishra, “A generic anti-QCD jet tagger,” *JHEP* **11** (2017) 163, [arXiv:1709.01087 \[hep-ph\]](#).
  - [6] A. Andreassen, B. Nachman, and D. Shih, “Simulation Assisted Likelihood-free Anomaly Detection,” *Phys. Rev. D* **101** no. 9, (2020) 095004, [arXiv:2001.05001 \[hep-ph\]](#).
  - [7] **ATLAS** Collaboration, G. Aad *et al.*, “Dijet resonance search with weak supervision using  $\sqrt{s} = 13$  TeV  $pp$  collisions in the ATLAS detector,” [arXiv:2005.02983 \[hep-ex\]](#).
  - [8] B. M. Dillon, D. A. Faroughy, and J. F. Kamenik, “Uncovering latent jet substructure,”

- Phys. Rev. D* **100** no. 5, (2019) 056002, [arXiv:1904.04200 \[hep-ph\]](#).
- [9] B. M. Dillon, D. A. Faroughy, J. F. Kamenik, and M. Szewc, “Learning the latent structure of collider events,” [arXiv:2005.12319 \[hep-ph\]](#).
- [10] O. Amram and C. M. Suarez, “Tag N’ Train: A Technique to Train Improved Classifiers on Unlabeled Data,” [arXiv:2002.12376 \[hep-ph\]](#).
- [11] M. C. Romao, N. Castro, and R. Pedro, “Finding New Physics without learning about it: Anomaly Detection as a tool for Searches at Colliders,” [arXiv:2006.05432 \[hep-ph\]](#).
- [12] T. Heimel, G. Kasieczka, T. Plehn, and J. M. Thompson, “QCD or What?,” *SciPost Phys.* **6** no. 3, (2019) 030, [arXiv:1808.08979 \[hep-ph\]](#).
- [13] M. Farina, Y. Nakai, and D. Shih, “Searching for New Physics with Deep Autoencoders,” [arXiv:1808.08992 \[hep-ph\]](#).
- [14] T. S. Roy and A. H. Vijay, “A robust anomaly finder based on autoencoder,” [arXiv:1903.02032 \[hep-ph\]](#).
- [15] A. Blance, M. Spannowsky, and P. Waite, “Adversarially-trained autoencoders for robust unsupervised new physics searches,” *JHEP* **10** (2019) 047, [arXiv:1905.10384 \[hep-ph\]](#).
- [16] O. Cerri, T. Q. Nguyen, M. Pierini, M. Spiropulu, and J.-R. Vlimant, “Variational Autoencoders for New Physics Mining at the Large Hadron Collider,” *JHEP* **05** (2019) 036, [arXiv:1811.10276 \[hep-ex\]](#).
- [17] D. P. Kingma and M. Welling, “Auto-Encoding Variational Bayes,” *arXiv e-prints* (Dec, 2013) [arXiv:1312.6114](#), [arXiv:1312.6114 \[stat.ML\]](#).
- [18] E. Nalisnick, A. Matsukawa, Y. Whye Teh, D. Gorur, and B. Lakshminarayanan, “Do Deep Generative Models Know What They Don’t Know?,” *arXiv e-prints* (Oct, 2018) [arXiv:1810.09136](#), [arXiv:1810.09136 \[stat.ML\]](#).
- [19] D. Hendrycks, M. Mazeika, and T. Dietterich, “Deep Anomaly Detection with Outlier Exposure,” *arXiv e-prints* (Dec, 2018) [arXiv:1812.04606](#), [arXiv:1812.04606 \[cs.LG\]](#).
- [20] G. Kasieczka and D. Shih, “DisCo Fever: Robust Networks Through Distance Correlation,” [arXiv:2001.05310 \[hep-ph\]](#).
- [21] **ATLAS Collaboration** Collaboration, “Performance of mass-decorrelated jet substructure observables for hadronic two-body decay tagging in ATLAS,” Tech. Rep. ATL-PHYS-PUB-2018-014, CERN, Geneva, Jul, 2018. <https://cds.cern.ch/record/2630973>.

- [22] L. Bradshaw, R. K. Mishra, A. Mitridate, and B. Ostdiek, “Mass Agnostic Jet Taggers,” *SciPost Phys.* **8** no. 1, (2020) 011, [arXiv:1908.08959 \[hep-ph\]](#).
- [23] C. Doersch, “Tutorial on Variational Autoencoders,” *arXiv e-prints* (June, 2016) [arXiv:1606.05908](#), [arXiv:1606.05908 \[stat.ML\]](#).
- [24] J. Alwall, M. Herquet, F. Maltoni, O. Mattelaer, and T. Stelzer, “Madgraph 5: going beyond,” *Journal of High Energy Physics* **2011** no. 6, (Jun, 2011) . [http://dx.doi.org/10.1007/JHEP06\(2011\)128](http://dx.doi.org/10.1007/JHEP06(2011)128).
- [25] T. Sjstrand, S. Mrenna, and P. Skands, “A brief introduction to pythia 8.1,” *Computer Physics Communications* **178** no. 11, (Jun, 2008) 852867. <http://dx.doi.org/10.1016/j.cpc.2008.01.036>.
- [26] J. de Favereau, C. Delaere, P. Demin, A. Giammanco, V. Lematre, A. Mertens, and M. Selvaggi, “Delphes 3: a modular framework for fast simulation of a generic collider experiment,” *Journal of High Energy Physics* **2014** no. 2, (Feb, 2014) . [http://dx.doi.org/10.1007/JHEP02\(2014\)057](http://dx.doi.org/10.1007/JHEP02(2014)057).
- [27] M. Cacciari, G. P. Salam, and G. Soyez, “The anti-kt jet clustering algorithm,” *Journal of High Energy Physics* **2008** no. 04, (Apr, 2008) 063063. <http://dx.doi.org/10.1088/1126-6708/2008/04/063>.
- [28] I. Higgins, L. Matthey, A. Pal, C. Burgess, X. Glorot, M. M. Botvinick, S. Mohamed, and A. Lerchner, “beta-vae: Learning basic visual concepts with a constrained variational framework,” in *ICLR*. 2017.
- [29] D. P. Kingma and J. Ba, “Adam: A method for stochastic optimization,” 2014.
- [30] L. van der Maaten and G. Hinton, “Visualizing data using t-SNE,” *Journal of Machine Learning Research* **9** (2008) 2579–2605. <http://www.jmlr.org/papers/v9/vandermaaten08a.html>.
- [31] T. Cheng, “Test sets for jet anomaly detection at the lhc,” June, 2020. <https://doi.org/10.5281/zenodo.3901833>.
- [32] G. Branco, P. Ferreira, L. Lavoura, M. Rebelo, M. Sher, and J. P. Silva, “Theory and phenomenology of two-Higgs-doublet models,” *Phys. Rept.* **516** (2012) 1–102, [arXiv:1106.0034 \[hep-ph\]](#).
- [33] P. T. Komiske, E. M. Metodiev, and J. Thaler, “Metric Space of Collider Events,” *Phys. Rev. Lett.* **123** no. 4, (2019) 041801, [arXiv:1902.02346 \[hep-ph\]](#).

- [34] C. Shimmin, P. Sadowski, P. Baldi, E. Weik, D. Whiteson, E. Goul, and A. Sgaard, “Decorrelated Jet Substructure Tagging using Adversarial Neural Networks,” *Phys. Rev. D* **96** no. 7, (2017) 074034, [arXiv:1703.03507 \[hep-ex\]](#).
- [35] G. Louppe, M. Kagan, and K. Cranmer, “Learning to Pivot with Adversarial Networks,” [arXiv:1611.01046 \[stat.ML\]](#).
- [36] G. J. Székely, M. L. Rizzo, and N. K. Bakirov, “Measuring and testing dependence by correlation of distances,” *arXiv e-prints* (Mar., 2008) arXiv:0803.4101, [arXiv:0803.4101 \[math.ST\]](#).
- [37] T. Cheng, “Interpretability Study on Deep Learning for Jet Physics at the Large Hadron Collider,” in *33rd Annual Conference on Neural Information Processing Systems*. 11, 2019. [arXiv:1911.01872 \[hep-ph\]](#).